Structural insights into the p97-Ufd1-Npl4 complex

Valerie E. Pye*, Fabienne Beuron*†, Catherine A. Keetch‡, Ciaran McKeown*, Carol V. Robinson‡, Hemmo H. Meyer§, Xiaodong Zhang*¶, and Paul S. Freemont*¶

*Division of Molecular Biosciences, Faculty of Natural Sciences, Imperial College London, London SW7 2AZ, United Kingdom; ‡Department of Chemistry, University of Cambridge, Lensfield Road, Cambridge, CB2 1EW, United Kingdom; and §Institute of Biochemistry, Eidgenössiche Technische Hochschule Zurich, 8093 Zurich, Switzerland

Edited by Jeffrey Brodsky, University of Pittsburgh, Pittsburgh, PA, and accepted by the Editorial Board November 8, 2006 (received for review April 26, 2006)

p97/VCP (Cdc48 in yeast) is an essential and abundant member of the AAA+ family of ATPases and is involved in a number of diverse cellular pathways through interactions with different adaptor proteins. The two most characterized adaptors for p97 are p47 and the Ufd1 (ubiquitin fusion degradation 1)-Npl4 (nuclear protein localization 4) complex. p47 directs p97 to membrane fusion events and has been shown to be involved in protein degradation. The Ufd1-Npl4 complex directs p97 to an essential role in endoplasmic reticulum-associated degradation and an important role in mitotic spindle disassembly postmitosis. Here we describe the structural features of the Ufd1-Npl4 complex and its interaction with p97 with the aid of EM and other biophysical techniques. The Ufd1-Npl4 heterodimer has an elongated bilobed structure that is ≈80 × 30 Å in dimension. One Ufd1-Npl4 heterodimer is shown to interact with one p97 hexamer to form the p97-Ufd1-Npl4 complex. The Ufd1-Npl4 heterodimer emanates from one region on the periphery of the N-D1 plane of the p97 hexamer. Intriguingly, the p97-p47 and the p97-Ufd1-Npl4 complexes are significantly different in stoichiometry, symmetry, and quaternary arrangement, reflecting their specific actions and their ability to interact with additional cofactors that cooperate with p97 in diverse cellular pathways.

AAA ATPase | adaptor complex | ubiquitin | protein degradation | EM

The AAA ATPase p97 (also known as VCP; Cdc48 in yeast) is involved in a plethora of cellular activities mediated via different adaptor proteins (see ref. 1 for review). p97 has two major mutually exclusive adaptors, p47 and the Ufd1 (ubiquitin fusion degradation 1)-Npl4 (nuclear protein localization 4) complex (2), that direct p97 to different cellular functions. The Ufd1-Npl4 complex was first isolated from rat liver cytosol, where it is present either as a heterodimer or bound to p97 (2). Ufd1 (34.5 kDa) had been previously identified in a yeast screen for mutants that failed to degrade a fusion protein with a nonremovable ubiquitin moiety (3), whereas Npl4 (68 kDa) was identified in a screen for mutants deficient in nuclear transport (4). This finding suggested that the Ufd1-Npl4 complex might link ubiquitination events with nuclear transport processes. The p97-Ufd1-Npl4 complex has been implicated in the regulation of spindle disassembly at the end of mitosis (5), centromere targeting (6), nuclear envelope reassembly postmitosis (7), and the regulation of a specific ubiquitylated transcription factor in yeast (8).

However, p97-Ufd1-Npl4 is also essential in an unrelated cellular pathway termed ERAD (endoplasmic reticulum-associated degradation), in which irreversibly misfolded or short-lived polypeptides from the ER are conjugated with ubiquitin and degraded/recycled by the 26S proteasome. p97-Ufd1-Npl4 has been shown to interact with ERAD substrates at the cytosolic side of the ER membrane recognizing 1-2 ubiquitins (9) covalently linked to substrate proteins via E1-E3 ubiquitin-conjugating enzymes (9–11). It is postulated that p97-Ufd1-Npl4 retrotranslocates substrate proteins out of the ER membrane into the cytosol (12) and is physically linked via membrane-bound factors (VIMP in mammals and Ubx2 in yeast) to the ubiquitination machinery and putative translocation pore (13–15). This function therefore suggests a requirement for p97 to accommodate and coordinate additional binding factors alongside Ufd1-Npl4.

The other major p97 adaptor, p47, directs p97 to both membrane fusion events (16) and protein degradation other than ERAD (14, 17). A wealth of structural information has already been obtained for p47 (18–20). In comparison, little is known about the structure of the Ufd1-Npl4 complex and its interaction with p97. Ufd1 has two functional domains (7), an N-terminal "UT3" domain recently solved by NMR (21) and a C-terminal "UT6" domain. As predicted (22, 23), UT3 is structurally similar to the p97 N domain, despite a lack of sequence identity, and comprises two independent binding sites for mono- and di/poly-ubiquitin respectively (21, 24). The UT6 domain is predicted to be unstructured and forms interactions with both Npl4 and p97 (7). Structurally, Npl4 has a C-terminal zinc finger domain that interacts with ubiquitin (25–27) (absent in yeast Npl4) and is predicted to have a ubiquitin-like N-terminal domain (UBD), which has been shown to interact with p97 when isolated from full-length Npl4 (28). Interestingly all three components of the p97-Ufd1-Npl4 complex have been shown to interact with various forms of ubiquitin (7, 8, 21, 24, 29). However, in the absence of any structural information on the ternary organization of the complex, it is difficult to reconcile the mode of ubiquitin binding with protein target recognition. Given the size of p97-Ufd1-Npl4 (≈650 kDa) and technical difficulties in reconstituting large complexes *in vitro*, we have applied single particle EM and biophysical methods to analyze the quaternary organization of the p97-Ufd1-Npl4 complex. We report the first low-resolution images of full-length Ufd1-Npl4, p97-Ufd1-Npl4 alone and in association with ubiquitin. Our studies allow insights into the spatial organization of p97-Ufd1-Npl4, which intriguingly is significantly different from the p97-p47 complex. Our results provide an explanation for how p97-Ufd1-Npl4 could interact with additional cofactors required in mediating ERAD.

Results

The Ufd1-Npl4 Heterodimer Has an Elongated Morphology. The stoichiometry of the Ufd1-Npl4 complex has previously been de-

Author contributions: V.E.P. and F.B. contributed equally to this work; V.E.P., F.B., C.V.R., H.H.M., X.Z., and P.S.F. designed research; V.E.P., F.B., C.A.K., and C.M. performed research; V.E.P., F.B., C.A.K., C.V.R., and H.H.M. contributed new reagents/analytic tools; V.E.P., F.B., C.A.K., C.V.R., X.Z., and P.S.F. analyzed data; and V.E.P., F.B., C.A.K., C.M., C.V.R., H.H.M., X.Z., and P.S.F. wrote the paper.

The authors declare no conflict of interest.

This article is a PNAS direct submission. J.B. is a guest editor invited by the Editorial Board.

Freely available online through the PNAS open access option.

Abbreviations: ERAD, endoplasmic reticulum-associated degradation; STEM, scanning transmission EM.

†Present address: Section of Structural Biology, The Institute of Cancer Research, Chester Beatty Laboratories, 237 Fulham Road, London SW3 6JB, United Kingdom.

¶To whom correspondence may be addressed. E-mail: xiaodong.zhang@imperial.ac.uk or p.freemont@imperial.ac.uk.

This article contains supporting information online at www.pnas.org/cgi/content/full/0603408104/DC1.

BIOCHEMISTRY

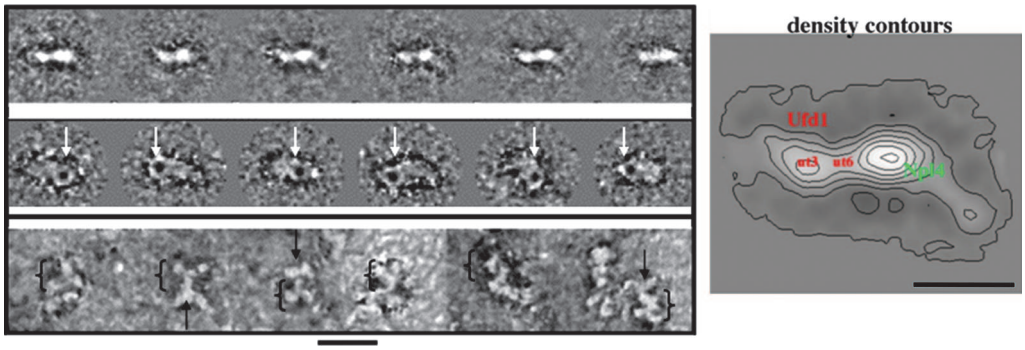

Fig. 1. Visualization of the Ufd1-Npl4 complex by cryo- and negative stain EM. (*Left Top*) Class averages of frozen, hydrated Ufd1-Npl4 complex (each class contains ≈20 aligned images). (*Left Middle*) Negatively stained Ufd1-Npl4 single particles labeled with NiNTA-nanogold particles directed to the C-terminal His_6-tag of Ufd1. One gold bead is present per complex (arrows). (*Left Bottom*) Ufd1-Npl4 was incubated with monoclonal IgGs directed against the N-terminal UT3 fragment of Ufd1. The antibody (indicated with a bracket) is binding the elongated particle close to its center (arrows). (*Right*) Average of 300 particles obtained by cryo-EM with superimposed density contours and a putative domain mapping. The protein is shown in white. (Scale bars: 5 nm.)

termined by multiangle laser light scattering to be a 1:1 ratio (≈100 kDa complex) (28). However, purified Ufd1-Npl4 runs at an apparent molecular mass of 200 kDa by size exclusion chromatography, suggesting a 2:2 complex or nonspherical shape (2). We wanted to further confirm the stoichiometry of the complex by using electrospray ionization MS. A major species with mass of 103.1 kDa and two minor species with masses of 34.8 and 68.1 kDa were observed. These masses correspond to the Ufd1-Npl4 complex, the Ufd1 monomer, and the Npl4 monomer, respectively [see supporting information (SI) Fig. 5*B Top*]. No peaks corresponding to a 2:2 or 3:3 complex were observed, establishing a 1:1 ratio for the complex. We also analyzed truncated versions of the complex by electrospray ionization MS. Both UT6-Npl4 and Ufd1-Npl4ΔZF were found to be a 1:1 complex, concluding that neither the UT3 domain of Ufd1 nor the zinc finger domain of Npl4 are required for or influence complex formation (SI Fig. 5*B Middle* and *Bottom*). The discrepancy between the actual mass of the complex and the apparent mass by size exclusion chromatography suggests that the Ufd1-Npl4 complex has a nonspherical shape.

We next attempted to visualize the Ufd1-Npl4 complex using EM to provide a low-resolution view of the native arrangement of the complex. Although negative stain can provide better contrast, we were able to obtain images of Ufd1-Npl4 using cryo-EM that directly images the protein complex. We viewed a homogeneous population of thin, elongated particles that we assumed to be Ufd1-Npl4 (Fig. 1 *Left Top*). To confirm that these particles were Ufd1-Npl4, we used three techniques. First, we used NiNTA-nanogold to label the C-terminal His_6-tag of Ufd1 and viewed the complex using negative stain EM (Fig. 1 *Left Middle*). One NiNTA-nanogold bead is observed per particle superimposed with one lobe of density. Second, we used a monoclonal antibody directed against the region between the subdomains of Ufd1 (amino acids 211–220) and found that it recognized an epitope located in the middle of the Ufd1-Npl4 particle (Fig. 1 *Left Bottom*). In these experiments, we used negative stain (higher signal-to-noise ratio than cryo-EM), which allowed us to more clearly observe single particles. Lastly, the Ufd1-Npl4 complex was analyzed by scanning transmission EM (STEM). STEM allows imaging and mass measurements of single particles. The dark-field signal in STEM is directly proportional to the local mass per unit area in the corresponding region of the specimen. Given absolute scattering cross-sections, intensity in the STEM can be integrated over an isolated particle and converted to a molecular weight (30). A total of 800 particles (typical dark-field image shown in SI Fig. 6*A*) were picked and their masses were measured by using the PCMass software. The resulting histogram (SI Fig. 6*B*) shows a maximum at a mass of ≈100 kDa, indicating that these particles are consistent with the Ufd1-Npl4 complex. The nanogold and antibody labeling together with STEM dark-field micrographs show unambiguously that the elongated particles analyzed by cryo-EM are the heterodimeric Ufd1-Npl4 complex.

We proceeded to analyze the 100-kDa complex and obtained 2D averages that show a bilobed structure with an overall length of ≈80 Å and a width of ≈30 Å (Fig. 1 *Right*). These two lobes exhibit different densities that are proportional to the molecular weight of the two components. The larger of the lobes we have attributed to Npl4, because this is the largest mass in the complex. There appears to be a flexible region between the two lobes, which we tentatively assign to the Ufd1 UT6 domain because this region interacts with Npl4. This region is also labeled by gold (directed to the C-terminal His_6-tag of Ufd1) and monoclonal antibodies (directed to the region between Ufd1 subdomains; Fig. 1). By elimination, we tentatively assign the Ufd1 UT3 domain to the smaller lobe, which has dimensions (≈40 × 40 Å) that are consistent with the UT3 structure (21).

Stoichiometry and Spatial Organization of the p97-Ufd1-Npl4 Complex. We next wanted to establish the stoichiometry of the p97-Ufd1-Npl4 complex. Previously, this complex had been suggested by analogy with the p97-p47 complex (16, 31) to be one p97 hexamer to three Ufd1-Npl4s (2, 8). Purified p97 alone and the p97-Ufd1-Npl4 complex were analyzed by STEM. For the p97 reference sample, 264 particles were picked and subsequently showed a distribution of masses peaking at ≈550 kDa, which corresponds well to p97 (534 kDa). For the p97-Ufd1-Npl4 sample, 495 particles were picked and led to a distribution of masses with a maximum at ≈650 kDa (SI Fig. 6*C*). The increase in mass of ≈100 kDa for the complex is consistent with one Ufd1-Npl4 heterodimer binding to one p97 hexamer. These results are also in agreement with previous gel filtration studies (7).

We next visualized the p97-Ufd1-Npl4 complex by negative stain EM. The complexes were easily identified because they exhibited an additional projection at the periphery of the p97 hexamer (Fig. 2*A*). A class average of 400 particles was calculated from a group of small subclasses showing apparent similar handedness of the p97 hexamer. The appendage visible on single particles (viewed from the top) emanates from a single region on the p97 hexamer and appears to comprise several domains (Fig. 2*B*). The diameter of the hexamer is ≈120 Å as previously reported on 2D averages (32). The additional mass has an elongated bilobed shape consistent with the dimensions of Ufd1-Npl4 (colored yellow in Fig. 2*B Right*). The density of one

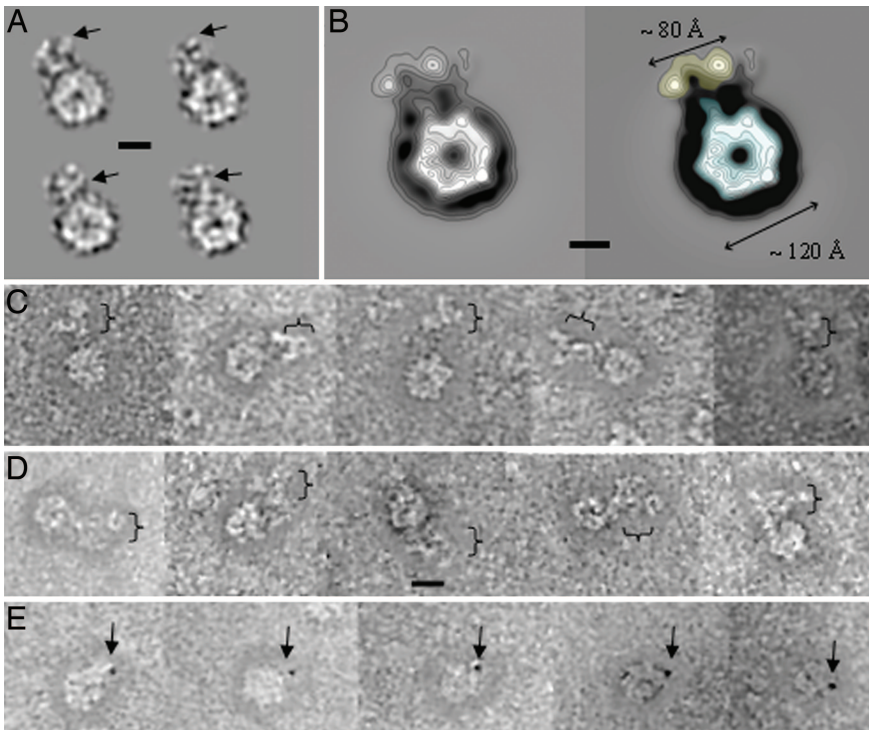

Fig. 2. Visualization of the p97-Ufd1-Npl4 complex by negative stain EM. (*A*) Single particles of negatively stained p97-Ufd1-Npl4 complex viewed down the p97 6-fold axis. An appendage is found at the periphery of p97 (arrow). (*B Left*) Class average of 400 particles band-pass filtered to 25 Å and shown with superimposed isodensity contours. (*Right*) The additional density has the size and shape of the Ufd1-Npl4 complex (yellow). The Ufd1-Npl4 density emanates from one peripheral point on the p97 top view. (*C*) Gallery of immunocomplexes using purified IgG directed against the C-terminal zinc finger of Npl4. A single IgG (bracket) is observed bound to the p97-Ufd1-Npl4 complex. (*D*) Gallery of immunocomplexes obtained using a monoclonal antibody against the N-terminal fragment of Ufd1. Similarly, a single IgG is bound per complex. (*E*) NiNTA-nanogold labeling of the C-terminal His_6-tag of Ufd1. One single gold bead (arrow) is observed per complex. (Scale bars: 5 nm.)

of the lobes appears slightly more prominent than the other. This asymmetry of the additional density, when compared with the Ufd1-Npl4 morphology, indicates that top and bottom views of p97 were not extensively mixed. This complex was also studied by cryo-EM but proved unsuccessful in identifying additional density on single p97 particles, probably because of the poorer contrast of this method.

To confirm that the observed appendage was indeed Ufd1-Npl4, we labeled the p97-Ufd1-Npl4 complex with each of the following: a purified IgG targeting the C-terminal zinc finger of Npl4, a monoclonal antibody targeting Ufd1, and NiNTA-nanogold to target the C-terminal His_6-tag of Ufd1. In the case of antibody labeling, both experiments resulted in the observation of a single antibody molecule per p97-Ufd1-Npl4 complex (Fig. 2 *C* and *D*). Similarly, with the gold labeling, a single NiNTA-nanogold particle was observed at the periphery of each p97 hexamer (Fig. 2*E*, black). All three independent labeling techniques confirm that only one Ufd1-Npl4 complex is bound per p97 hexamer and are consistent with the Ufd1-Npl4 complex emanating from a single region at the periphery of the p97 hexamer. These labeling studies also indicate that the zinc finger of Npl4 and the region between Ufd1 subdomains are both accessible when in complex with p97. The Ufd1 C-terminal His_6-tag is similarly exposed to bind an 18-Å gold particle, despite the C-terminal UT6 domain being involved in binding both the p97 N domain and Npl4.

p97-Ufd1-Npl4 Interactions with Ubiquitin. The p97-Ufd1-Npl4 complex interacts with ubiquitin to function in the ERAD pathway and possibly in mitotic spindle disassembly. The interaction mode and spatial arrangement of this complex would provide insights into the p97-Ufd1-Npl4-substrate interactions. However, ubiquitin is a small protein (8.6 kDa) and is virtually invisible when using EM techniques. Indeed p97-Ufd1-Npl4 incubated in the presence of excess tetra-ubiquitin and imaged by EM did not differ significantly from the p97-Ufd1-Npl4 projection average (data not shown). We therefore incubated the p97-Ufd1-Npl4 complex with ubiquitin-GST, which is significantly larger (dimer of 70 kDa) and imaged the resultant complex by EM (Fig. 3 *A–C*). The complex exhibited a single extradensity when compared with p97-Ufd1-Npl4 alone (Fig. 2*A*). The 2D average of 150 such complexes (Fig. 3*B*) shows an extension, ≈150 Å long, connected to p97. The total additional density comprises two main regions: one connected to p97 by a region assumed to be a p97 N domain and one formed of a more globular domain joined with additional mass. The latter has dimensions consistent with a GST dimer (Fig. 3*C Inset*). The region that is connected to p97 has an overall length of ≈80 Å, and we attribute this density to the Ufd1-Npl4 complex (Fig. 3*C*, yellow).

These data further confirm that one Ufd1-Npl4 is bound at the periphery of a p97 hexamer and shows that the ubiquitin-GST is found adjacent to the Ufd1-Npl4 complex. We also obtained a 2D average of p97-Ufd1-Npl4ΔZF-ubiquitin-GST (Fig. 3*D*) which is very similar to the p97-Ufd1-Npl4-ubiquitin-GST complex, indicating that ubiquitin-GST binds to the Ufd1 UT3 domain and not the Npl4 zinc finger. We found this finding surprising because Ufd1 has a lower affinity for mono-ubiquitin than the Npl4 zinc finger (21, 25, 27). To confirm these observations, we also incubated p97-UT6-Npl4 with ubiquitin-GST and analyzed these particles by EM. We did not observe any additional density for ubiquitin-GST (data not shown), support-

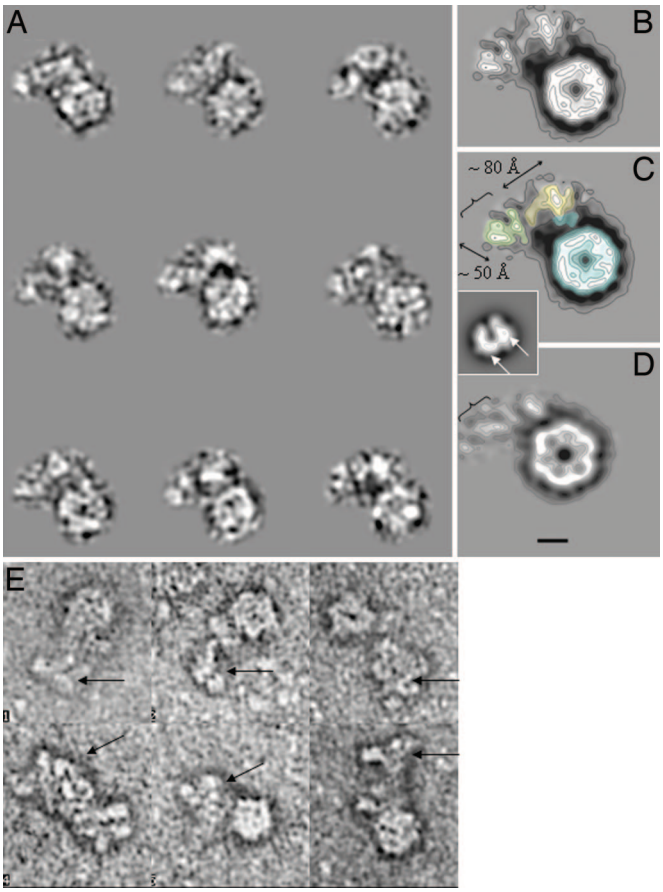

Fig. 3. Visualization of p97-Ufd1-Npl4-ubiquitin complexes by negative stain EM. (*A*) Band pass filtered images of the p97-Ufd1-Npl4-ubiquitin-GST complexes showing top views of p97 with a significant elongated extra-density at the periphery. (*B*) Class average of 150 p97-Ufd1-Npl4-ubiquitin-GST particles band-pass filtered to 25 Å and shown with superimposed iso-density contours. (*C*) Same average with overlaid yellow to mark the putative Ufd1-Npl4 complex, green for the ubiquitin-GST [*Inset* shows crystal structure of a GST dimer (PDB ID code 1PKZ) filtered to 25-Å resolution and viewed in an orientation matching the EM average] and in blue the p97 top view with the p97 N domain bound to the Ufd1-Npl4 complex. (*D*) Average of 150 top views of p97-Ufd1-Npl4ΔZF-ubiquitin-GST with superimposed density contours showing a similar domain organization to the Ufd1-Npl4-ubiquitin-GST bound to p97, in particular the GST moiety (bracket). (*E*) Gallery of p97-Ufd1-Npl4-ubiquitin (3–7 moieties, K48-linked) complexes incubated with an excess of purified IgGs (arrows) directed against ubiquitin. (Scale bar: 5 nm.)

ing the notion that ubiquitin-GST can bind the Ufd1 UT3 domain. In addition, when we incubated the p97-Ufd1-Npl4-ubiquitin-GST complex with an excess of mono-ubiquitin, the ubiquitin-GST appears to dissociate from the p97-Ufd1-Npl4 complex, consistent with the ubiquitin moiety of the GST fusion protein being responsible for the interaction with p97-Ufd1-Npl4 (SI Fig. 7). The different orientation of the p97-Ufd1-Npl4ΔZF-ubiquitin-GST particles on the carbon support film, compared with full-length complex, is likely responsible for the better definition of the p97 hexamer and the different projection angle (not as elongated as in Fig. 3*B*).

Finally, the p97-Ufd1-Npl4 complexes were incubated with an excess of K48-linked poly-ubiquitin (3–7 moieties) and labeled with an IgG directed against ubiquitin. These particles clearly show the ubiquitin chain binding to the p97-Ufd1-Npl4 complex via Ufd1-Npl4 (Fig. 3*E*).

Discussion

Comparison of Adaptor Proteins: p47 vs. Ufd1-Npl4. The two major adaptors for the AAA ATPase p97, p47 and Ufd1-Npl4, have previously been shown to bind to p97 via a common bipartite mechanism (28). However, p47 and Ufd1-Npl4 remain distinct. The first structural view of Ufd1-Npl4, reported here, shows a bilobed elongated particle. We have tentatively assigned positions of the Ufd1-Npl4 domains in our projection structure based on size of density and labeling studies with nanogold and antibody. In comparison, p47 has three well defined domains (18–20, 33) separated by long linkers and is a trimer in solution (19, 31). Despite p47 (≈150 kDa) being larger than the Ufd1-Npl4 complex, it is not readily visualized by EM (data not shown), probably because of the inherent flexibility of the individual domains. However, p47 is readily identified by EM when bound to p97 and is located on top of the p97 hexamer (16, 31). Long flexible linkers between the p47 domains are thought to be key in transmitting energy from p97 ATP binding and hydrolysis to potential target substrates. Interestingly, the p97-Ufd1-Npl4 complex is very different from the p97-p47 complex. First, Ufd1-Npl4 is a 1:1 complex and has no higher-order oligomeric state formed in solution. Second, only one Ufd1-Npl4 complex binds per p97 hexamer, resulting in a nonsymmetrical complex. Finally, the Ufd1-Npl4 complex appears to project out from the main body of p97, although it is possible that we have captured a single conformation by our EM approach. Nevertheless, both complexes are sufficiently distinct, which leads to the questions as to why a single Ufd1-Npl4 complex binds to p97?

One possibility is that binding of Ufd1-Npl4 induces conformational changes that inhibit further Ufd1-Npl4 complexes from binding, possibly relocating the bound N domain such that the other N domains are rearranged. For an effective p97-Ufd1-Npl4 complex to be formed, binding of Ufd1-Npl4 must induce some form of allosteric effect to the other p97 N domains to make them available or even promote further adaptor binding (Fig. 4). Consistent with this notion is the finding that Ufd1-Npl4 and Ubx2, the membrane anchor of p97 during ERAD in yeast (14, 15), can bind to a single 97 hexamer. Our results support the concept of p97 binding different cofactors simultaneously.

Ubiquitin Binding to p97-Ufd1-Npl4. Each entity within the p97-Ufd1-Npl4 complex has at least one ubiquitin recognition motif allowing for potential multiple ubiquitin binding events. Recently, the atomic resolution structure of the UT3 domain of Ufd1 has been reported and two distinct ubiquitin interacting surfaces were mapped, one for mono-ubiquitin and the other for K48-linked poly-ubiquitin (21). We observe both mono- and poly-ubiquitin binding at a similar location within Ufd1-Npl4 complex. Both ubiquitin binding sites seem to be available for binding in the full-length complex, consistent with the results of Park *et al.* (21). It has been shown *in vivo* that the UT3 ubiquitin-binding domain is crucial for ERAD (24). Supporting these studies, we visualized one mono-ubiquitin molecule/K48-linked poly-ubiquitin chain binding to p97-Ufd1-Npl4, and our results suggest that these interactions occur via the Ufd1 UT3 domain. There was no evidence for further ubiquitin binding to p97 or to the Npl4 zinc finger as previously shown (8, 25, 26, 29), although it is available for interactions within the complex studied here as seen by antibody labeling. The binding of ubiquitin to Ufd1 in preference to Npl4 in solution (shown here) may be reflective of the different experimental conditions when compared with previous pull-down assays (25). p97 has also been reported to bind ubiquitin with a preference for K48-linked chains (8, 29). Although we do not observe additional ubiquitin binding to p97, we cannot rule out additional recognition by p97 of the K48-linked poly-ubiquitin chain once bound.

The ubiquitin interaction sites on p97 have been predicted to be similar to those on the UT3 domain of Ufd1, because they both exhibit a similar fold despite their low sequence homology (21). To locate these sites in the context of the p97 hexamer, we superimposed the UT3 domain onto a p97 N domain. The region

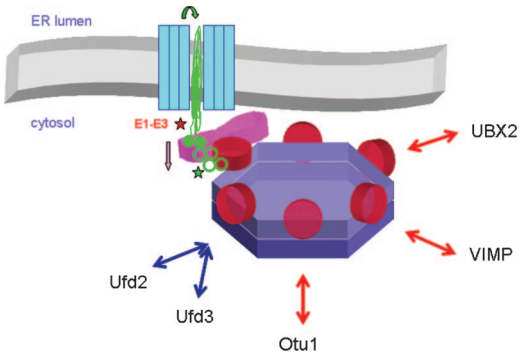

Fig. 4. Schematic summary of the spatial arrangement of p97-Ufd1-Npl4 in the ERAD pathway. The ER membrane (wavy gray line) hosts numerous transmembrane proteins that could be potential sites for the retrotranslocation of ERAD substrates (represented as blue rectangles). p97 D1 D2 domains are represented as purple hexagons, and N domains are represented as red cylinders. Ufd1-Npl4 is represented as a pink bilobe shape, which we suggest is interacting with a p97 N domain via its thinnest central region. We speculate that the binding of one Ufd1-Npl4 complex to p97 causes a rearrangement of other N domains to prevent further Ufd1-Npl4 binding and to promote interactions with other proteins (represented by different orientation of ''red cylinder'' N domains and red arrows). Membrane-bound proteins that have been shown to bind p97-Ufd1-Npl4 via p97 N domains are VIMP in mammals (13) and Ubx2 in yeast (14, 15). In yeast, p97-Ufd1-Npl4 can also interact with the E4 ligase, Ufd2 (in competition with Ufd3) via p97ΔN (blue arrows) (9, 43), and the deubiquitinating enzyme, Otu1 (simultaneously with Ufd3) via the p97 N domain (43). p97-Ufd1-Npl4 recognizes the ERAD substrate via 1-2 ubiquitin moieties (green circles) (9) at one region of Ufd1-Npl4 (UT3 domain). The green ''fuzz'' represents the ERAD substrate which may also interact with p97 itself. The green arrow represents recognition and movement of the ERAD substrate from the lumen to the cytosolic face of the ER. The red star represents the action of the E1-E3 enzymes on the ERAD substrate, covalently attaching ubiquitin moieties; the green star and green rings represent the possibility of further ubiquitin moieties being added [e.g., by E4 enzyme, Ufd2 (9)] and interacting with the Ufd1-Npl4-bound p97 N domain (although interactions with other N domains are not excluded). The action of the p97-Ufd1-Npl4 complex ''pulling'' the substrate into the cytosol (pink arrow) is essential for the delivery of the ERAD substrate to the 26S proteasome. Figure is not to drawn scale.

attributed to poly-ubiquitin recognition is situated on the underside of the N domain adjacent to the cleft responsible for p47 UBX domain binding (33) and proposed Ufd1-Npl4 recognition (28). The exposed position on p97 of the postulated poly-ubiquitin recognition site allows ample space for attached substrates to be located peripheral to the p97 hexamer. This arrangement could allow simultaneous binding of poly-ubiquitin to both Ufd1-Npl4 and p97, enhancing the relative affinities of these interactions. When viewing the equivalent location of the Ufd1 UT3 mono-ubiquitin interaction site in p97, this region would be buried at the N-D1 interface and partially covered by the N-D1 linker. It is difficult to imagine how mono-ubiquitin could bind at this inaccessible site without considerable rearrangement of p97 N domains.

It would be attractive to think that a ubiquitin chain could interact with each p97 N domain in turn and encircle the p97 hexamer, thus limiting the ubiquitin chain to six moieties with one ubiquitin per N domain (9). However, based on available structural information, it appears that ubiquitin is too small to span from one p97 N domain to the next without extensive rearrangement of N domains. At least four K48-linked ubiquitins are required to span two adjacent p97 N domains as positioned in p97 crystal structures (33–37). It is perhaps more plausible that a poly-ubiquitin chain could interact with the p97-Ufd1-Npl4 complex via two similar interaction sites, on Ufd1 and p97, respectively, thereby allowing a longer ubiquitin chain to be associated with higher affinity. In comparison, p97-p47 is reported to bind preferentially mono-ubiquitin (25), although poly-ubiquitinated proteins have been shown to bind to the yeast homologue Shp1 *in vivo* (14). The difference in ubiquitin binding between both p97 adaptor complexes is likely to be functionally relevant. Although p47 binds to mono-ubiquitin moieties via the UBA domain (possibly up to three per complex), the location of this binding is likely to be far away from further possible p97-ubiquitin interactions (19, 31). In contrast, Ufd1-Npl4 can bind ubiquitin close to the body of p97, enabling a poly-ubiquitin chain to be associated with both Ufd1-Npl4 and p97 synergistically. These differences could reflect a requirement for different actions to be performed on ubiquitin moieties by p97 in different cellular pathways.

Methods

Protein Expression and Purification. All proteins used were expressed in *Escherichia coli* Rosetta (DE3) cells using the following constructs: full-length p97(His_6) (35), Ufd1(His_6) (2, 25), untagged Npl4 (2, 25), (His_6)UT6 (2, 25), untagged Npl4ΔZF (25), untagged p97 [kindly provided by Hisao Kondo (31)], and ubiquitin-GST (25) as described previously. Protein complexes (with exception of ubiquitin-GST) were formed and purified by mixing appropriate amounts of clarified cell lysates that were then loaded onto a HiTrap chelating column (GE Healthcare, Bucks, U.K.) precharged with Ni^{2+}, and complexes were eluted from the column with an imidazole gradient according to the manufacturer's guidelines. Fractions were assessed for complex formation and purity by SDS/PAGE and were further purified by gel filtration (Superdex 200 16/60 prep grade or Superose 6 analytical grade; Amersham Biosciences) in buffer comprising 150 mM KCl, 25 mM Tris, 2.5 mM $MgCl_2$, 1 mM ATP, and 5% glycerol (pH 8.0) and concentrated to desired protein concentration in centricon modules (30,000 molecular weight cutoff; Amicon). For the p97-Ufd1-Npl4 complex, lysate containing untagged p97 was incubated with a large excess of prepurified Ufd1-Npl4 and purified by HiTrap affinity and gel filtration to ensure full occupation of p97 by Ufd1-Npl4 (SI Fig. 8). Ubiquitin-GST was purified as described (25). p97-Ufd1-Npl4 at a concentration of ≈60 nM was incubated with ≈6 μM ubiquitin-GST at room temperature for 30 min. To compete off the ubiquitin-GST, this complex was further incubated with ≈100 μM mono-ubiquitin (Sigma-Aldrich, Dorset, U.K.). K48-linked poly-ubiquitin chains were purchased from Gentaur (Brussels, Belgium) and incubated with the p97-Ufd1-Npl4 at a molar excess before being incubated with the antibodies. Protein concentrations were assessed by measuring the absorbance at 280 nm and background absorbance was corrected with a 240–360 nm scan. Protein complexes were confirmed by gel filtration profile and comparison of SDS/PAGE with native-PAGE.

Mass Spectroscopy. The nano-electrospray mass spectra were recorded on a quadrupole TOF II MS (Micromass, Manchester, U.K.) equipped with a z-spray source. This instrument is modified for high-mass operation as described (38). To maintain noncovalent interactions, analyses were carried out under conditions of increased pressure in the mass spectrometer: ion transfer stage pressure, 1.13×10^{-2} mbar (1 bar = 100 kPa), and TOF analyzer pressure, 5.41×10^{-7} mbar. Nanoflow needles were made in house as described (39). The samples (70 mg/ml) were buffer exchanged into 200 mM ammonium acetate (pH 7.0) immediately before analysis using Micro Bio-Spin 6 columns (Bio-Rad Laboratories, Hercules, CA).

NiNTA-Nanogold Labeling. Purified Ufd1(His_6)-Npl4 diluted to ≈20 μg/ml in 150 mM KCl, 25 mM Tris, 2.5 mM $MgCl_2$, and 1 mM ATP (pH 8.0) were adsorbed onto a glow-discharged carbon-coated grid and incubated for 10 min with substoichio-

metric amounts of NiNTA-nanogold (Nanoprobes Inc., Yaphank, NY) marker. The grids were then rapidly washed with buffer followed by two drops of water and negatively stained in 1% uranyl acetate, blotted, and air dried.

Antibody Labeling. Monoclonal antibody against Ufd1 or purified, polyclonal IgG directed against the zinc finger of Npl4 (2) and polyclonal anti-ubiquitin IgGs (SIGMA) were used for antibody labeling of Ufd1-Npl4 and p97-Ufd1-Npl4 complexes. The protein complexes were incubated at room temperature for 30 min at a molar ratio of ≈2 IgG:Ufd1-Npl4. A glow-discharged copper grid supporting a continuous collodion-carbon film was placed onto a drop of the sample for 2 min. The grid was subsequently washed in buffer and water and negatively stained with 1% uranyl acetate, blotted, and air dried.

EM. ***Conventional transmission EM.*** For negative staining, samples (20–50 μg/ml) were adsorbed onto freshly glow-discharged carbon-coated grids, rinsed with water, and stained with 1% uranyl acetate. Micrographs were recorded on a T12 or a CM200 (FEI, Eindhoven, Netherlands) operating at 120 kV.

Cryo-EM. Drops (5 μl) of Ufd1-Npl4 sample were applied to washed glow-discharged copper grids supporting a lacey carbon film (Agar Scientific, Stansted, U.K.). The drop was blotted quickly with filter paper and quench-frozen in liquid ethane. The grid was then transferred into a Gatan 626 cryo-holder and inserted into the microscope (CM200; FEI). Micrographs were recorded at an accelerating voltage of 200 kV at a nominal magnification of 50,000× on Kodak (Rochester, NY) SO163 film under minimal electron dose illumination. Micrographs were digitized with a Leafscan 45 scanner (Leaf Systems Inc., Southborough, MA) to 2.6 Å per pixel.

STEM. Dark-field micrographs of freeze-dried specimen were recorded at 1.0 or 2.0 nm per pixel at the Brookhaven STEM resource (Brookhaven National Laboratory, Upton, NY). Mass measurements were performed by using the PCMass software. Tobacco mosaic virus particles served as a mass standard (131.4 kDa/nm) (40).

Two-dimensional averaging. Image processing was performed by using the IMAGIC-5 software (41). The centered (nonrotationally aligned) images were subjected to multivariate statistical analysis giving rise to a first set of averages. A first set of references was extracted after this first cycle of classification followed by several rounds of rotational and translational alignments. The final average was the sum of small subclasses showing a similar handedness for p97 and visible density for the Ufd1-Npl4 heterodimer. Only particles showing a significant additional mass in the p97-Ufd1-Npl4 +/−ubiquitin-GST top view population were selected, resulting in the class averages (Figs. 2 and 3).

Superposition of UT3 and p97 N Domain Structures. The closest to mean model of the UT3 NMR structure was chosen (model 1 in Protein Data Bank ID code 1ZNC; www.pdb.org) to be superimposed on the p97 structure (PDB ID code 1R7R). Residues 1–19 and 197-end were removed from the UT3 structure because they are disordered. LSQMAN (42) was used to superimpose the structures. Resultant superposition had a rmsd of 1.85 Å over 124 residues.

We are grateful to Trevor Huyton and Tony Shaw for their initial work on this project. We thank Ingrid Dreveny and Louise Briggs for fruitful discussions and critically reading the manuscript and Cecilia Bebeacua, Rivka Isaacson, Xuemei Yuan, and Steve Matthews for useful discussions. We are very grateful to Martha Simon at the Brookhaven STEM facility for collecting the STEM data and for useful discussions. We thank the Wellcome Trust for their generous funding. The Brookhaven National Laboratory STEM is a National Institutes of Health Supported Resource Center, NIH 5 P41 EB2181, with additional support provided by the Department of Energy and the Office of Biological and Environmental Research.

1. Dreveny I, Pye VE, Beuron F, Briggs LC, Isaacson RL, Matthews SJ, McKeown C, Yuan X, Zhang X, Freemont PS (2004) *Biochem Soc Trans* 32:715–720.
2. Meyer HH, Shorter JG, Seemann J, Pappin D, Warren G (2000) *EMBO J* 19:2181–2192.
3. Johnson ES, Ma PC, Ota IM, Varshavsky A (1995) *J Biol Chem* 270:17442–17456.
4. DeHoratius C, Silver PA (1996) *Mol Biol Cell* 7:1835–1855.
5. Cao K, Nakajima R, Meyer HH, Zheng Y (2003) *Cell* 115:355–367.
6. Vong QP, Cao K, Li HY, Iglesias PA, Zheng Y (2005) *Science* 310:1499–1504.
7. Hetzer M, Meyer HH, Walther TC, Bilbao-Cortes D, Warren G, Mattaj IW (2001) *Nat Cell Biol* 3:1086–1091.
8. Rape M, Hoppe T, Gorr I, Kalocay M, Richly H, Jentsch S (2001) *Cell* 107:667–677.
9. Richly H, Rape M, Braun S, Rumpf S, Hoege C, Jentsch S (2005) *Cell* 120:73–84.
10. Pickart CM, Eddins MJ (2004) *Biochim Biophys Acta* 1695:55–72.
11. Passmore LA, Barford D (2004) *Biochem J* 379:513–525.
12. Ye Y, Meyer HH, Rapoport TA (2001) *Nature* 414:652–656.
13. Ye Y, Shibata Y, Yun C, Ron D, Rapoport TA (2004) *Nature* 429:841–847.
14. Schuberth C, Richly H, Rumpf S, Buchberger A (2004) *EMBO Rep* 5:818–824.
15. Neuber O, Jarosch E, Volkwein C, Walter J, Sommer T (2005) *Nat Cell Biol* 7:993–998.
16. Kondo H, Rabouille C, Newman R, Levine TP, Pappin D, Freemont P, Warren G (1997) *Nature* 388:75–78.
17. Hartmann-Petersen R, Wallace M, Hofmann K, Koch G, Johnsen AH, Hendil KB, Gordon C (2004) *Curr Biol* 14:824–828.
18. Yuan X, Shaw A, Zhang X, Kondo H, Lally J, Freemont PS, Matthews S (2001) *J Mol Biol* 311:255–263.
19. Yuan X, Simpson P, McKeown C, Kondo H, Uchiyama K, Wallis R, Dreveny I, Keetch C, Zhang X, Robinson C, *et al.* (2004) *EMBO J* 23:1463–1473.
20. Soukenik M, Diehl A, Leidert M, Sievert V, Bussow K, Leitner D, Labudde D, Ball LJ, Lechner A, Nagler DK, Oschkinat H (2004) *FEBS Lett* 576:358–362.
21. Park S, Isaacson R, Kim HT, Silver PA, Wagner G (2005) *Structure (London)* 13:995–1005.
22. Coles M, Diercks T, Liermann J, Groger A, Rockel B, Baumeister W, Koretke KK, Lupas A, Peters J, Kessler H (1999) *Curr Biol* 9:1158–1168.
23. Golbik R, Lupas AN, Koretke KK, Baumeister W, Peters J (1999) *Biol Chem* 380:1049–1062.
24. Ye Y, Meyer HH, Rapoport TA (2003) *J Cell Biol* 162:71–84.
25. Meyer HH, Wang Y, Warren G (2002) *EMBO J* 21:5645–5652.
26. Wang B, Alam SL, Meyer HH, Payne M, Stemmler TL, Davis DR, Sundquist WI (2003) *J Biol Chem* 278:20225–20234.
27. Alam SL, Sun J, Payne M, Welch BD, Blake BK, Davis DR, Meyer HH, Emr SD, Sundquist WI (2004) *EMBO J* 23:1411–1421.
28. Bruderer RM, Brasseur C, Meyer HH (2004) *J Biol Chem* 279:49609–49616.
29. Dai RM, Li CC (2001) *Nat Cell Biol* 3:740–744.
30. Wall JS, Hainfeld JF, Simon MN (1998) *Methods Cell Biol* 53:139–164.
31. Beuron F, Dreveny I, Yuan X, Pye VE, Mckeown C, Briggs LC, Cliff MJ, Kaneko Y, Wallis R, Isaacson RL, *et al.* (2006) *EMBO J* 25:1967–1976.
32. Rouiller I, Butel VM, Latterich M, Milligan RA, Wilson-Kubalek EM (2000) *Mol Cell* 6:1485–1490.
33. Dreveny I, Kondo H, Uchiyama K, Shaw A, Zhang X, Freemont PS (2004) *EMBO J* 23:1030–1039.
34. Zhang X, Shaw A, Bates PA, Newman RH, Gowen B, Orlova E, Gorman MA, Kondo H, Dokurno P, Lally J, *et al.* (2000) *Mol Cell* 6:1473–1484.
35. Huyton T, Pye VE, Briggs LC, Flynn TC, Beuron F, Kondo H, Ma J, Zhang X, Freemont PS (2003) *J Struct Biol* 144:337–348.
36. DeLaBarre B, Brunger AT (2003) *Nat Struct Biol* 10:856–863.
37. DeLaBarre B, Brunger AT (2005) *J Mol Biol* 347:437–452.
38. Sobott F, Hernandez H, McCammon MG, Tito MA, Robinson CV (2002) *Anal Chem* 74:1402–1407.
39. Nettleton EJ, Sunde M, Lai Z, Kelly JW, Dobson CM, Robinson CV (1998) *J Mol Biol* 281:553–564.
40. Wall JS, Hainfeld JF (1986) *Annu Rev Biophys Biophys Chem* 15:355–376.
41. van Heel M, Harauz G, Orlova EV, Schmidt R, Schatz M (1996) *J Struct Biol* 116:17–24.
42. Kleywegt GJ, Jones TA (1994) *Joint CCP4/ESF-EACBM Newsletter on Protein Crystallography* (Daresbury Lab, Warrington, UK) 31:9–14.
43. Rumpf S, Jentsch S (2006) *Mol Cell* 21:261–269.